Air-Stable, Cross-Linkable, Hole-Injecting/Transporting Interlayers for Improved Charge Injection in Organic Light-Emitting Diodes

Jianfeng Li and Tobin J. Marks*

Department of Chemistry and the Materials Research Center, Northwestern University, 2145 Sheridan Road, Evanston, Illinois 60208

Received December 26, 2007. Revised Manuscript Received May 27, 2008

Modification of inorganic electrode surfaces has attracted great attention in the quest to optimize organic optoelectronic devices. An air-stable, cross-linkable trimethoxysilane functionalized hole-transporting triarylamine (4,4′-bis[(*p*-trimethoxysilylpropylphenyl)phenylamino]biphenyl, TPD−[Si(OMe)$_3$]$_2$) has been synthesized and self-assembled or spin-coated onto tin-doped indium oxide (ITO) anode surfaces to form monolayers or multilayer siloxane films, respectively. The modified ITO surfaces were characterized by advancing aqueous contact angle, X-ray photoelectron spectroscopy (XPS), atomic force microscopy (AFM), and cyclic voltammetry (CV). Increased surface work function and enhanced ITO−hole transport layer (HTL) contact via robust covalent bonding are expected to facilitate hole injection from the ITO anode, resulting in organic light-emitting diode (OLED) performance enhancement versus that of a device without such interlayers. For a device having the structure ITO/spin-coated-TPD−[Si(OMe)$_3$]$_2$ from aqueous alcohol + acetic acid blend solution (40 nm)/NPB (20 nm)/Alq (60 nm)/LiF (1 nm)/Al (100 nm), a maximum light output of 32 800 cd/m^2, a 4.25 V turn-on voltage, and a maximum current efficiency of 5.8 cd/A is achieved. This performance is comparable to or superior to that of analogous devices prepared with analogous trichorosilyl precursors. The air-stable interlayer material developed here is also applicable to large-area coating techniques.

1. Introduction

Small-molecule and polymer organic light-emitting diodes (OLEDs) show promise of revolutionizing display technology due to distinctive attractions over conventional cathode ray tube and liquid crystal displays such as lower materials cost, superior brightness and color purity, markedly lower drive voltages, as well as increased viewing angles.[1–7] Improving OLED electroluminescent characteristics has been the focus of an extensive worldwide research effort with notable success in both device fabrication techniques and materials development.[8–17] OLEDs are "dual-injection" devices in which holes and electrons are injected from the anode and cathode, respectively, under application of an electric field, into an active molecular/macromolecular medium. Some fraction of the electron−hole pairs recombine to form excitons, which in turn radiatively decay to ground states and emit light.[6,18] To achieve optimum device performance, it is desirable to have multilayer structures[5] having discrete hole transport layer (HTL),[19] emissive layer (EML), and electron-transport layer (ETL)[20] functions (Figure 1). With such multilayer structures, high-performance devices[8,12] have been realized for small-molecule-based OLEDs fabricated

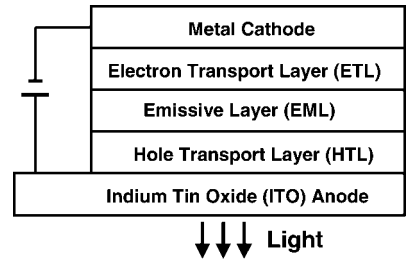

Figure 1. Cross section of a typical multilayer OLED structure.

* Corresponding author. E-mail: t-marks@northwestern.edu.

(1) Martin, G. In *Handbook of Optoelectronics*; Dakin, J. P., Brown, R. G. W., Eds.; CRC Press LLC: Boca Raton, FL, 2006; Vol. II, Chapter 1, pp 693−718.
(2) Veinot, J. G. C.; Marks, T. J. *Acc. Chem. Res.* **2005**, *38*, 632.
(3) Chen, C.-T. *Chem. Mater.* **2004**, *16*, 4389–4400.
(4) Shim, H.-K.; Jin, J.-I. *Adv. Polym. Sci.* **2002**, *158*, 193–243.
(5) Nalwa, H. S. In *Handbook of Advanced Electronic and Photonic Materials and Devices*; Nalwa, H. S., Ed.; Academic: San Diego, CA, 2001; Vol. 10, pp 1−51.
(6) Mitschke, U.; Baürle, P. *J. Mater. Chem.* **2000**, *10*, 1471–1507.
(7) Scherf, U.; List, E. J. W. *Adv. Mater.* **2002**, *14*, 477–489.
(8) Huang, Q.; Li, J.; Evmenenko, G. A.; Dutta, P.; Marks, T. J. *J. Appl. Phys.* **2007**, *101*, 093101/01.
(9) Huang, Q.; Li, J.; Evmenenko, G. A.; Dutta, P.; Marks, T. J. *Chem. Mater.* **2006**, *18*, 2431.
(10) Huang, Q.; Evmenenko, G. A.; Dutta, P.; Lee, P.; Armstrong, N. R.; Marks, T. J. *J. Am. Chem. Soc.* **2005**, *127*, 10227.
(11) Huang, Q.; Evmenenko, G.; Dutta, P.; Marks, T. J. *J. Am. Chem. Soc.* **2003**, *125*, 14704.
(12) Huang, Q. L.; Cui, J.; Veinot, J. G. C.; Yan, H.; Marks, T. J. *Appl. Phys. Lett.* **2003**, *82*, 331–333.
(13) Niu, Y. H.; Hou, Q.; Cao, Y. *Appl. Phys. Lett.* **2003**, *82*, 2163–2165.
(14) Duan, J. P.; Sun, P. P.; Cheng, C. H. *Adv. Mater.* **2003**, *15*, 224–227.
(15) Müller, C. D.; Falcou, A.; Reckefuss, N.; Rojahn, M.; Wiederhirn, V.; Rudati, P.; Frohne, H.; Nuyken, O.; Becker, H.; Meerholz, K. *Nature* **2003**, *421*, 829–833.
(16) Niu, Y. H.; Yang, W.; Cao, Y. *Appl. Phys. Lett.* **2002**, *81*, 2884–2886.
(17) Herguch, P.; Jiang, X. Z.; Liu, M. S.; Jen, A. K. Y. *Macromolecules* **2002**, *35*, 6094–6100.
(18) Ishii, H.; Sugiyama, K.; Ito, E.; Seki, K. *Adv. Mater.* **1999**, *11*, 605–625.
(19) Tang, C. W.; VanSlyke, S. A. *Appl. Phys. Lett.* **1987**, *51*, 913–915.
(20) Brown, A. R.; Bradley, D. D. C.; Burroughes, J. H.; Friend, R. H.; Greenham, N. C.; Burn, P. L.; Holmes, A. B.; Kraft, A. *Appl. Phys. Lett.* **1992**, *61*, 2793–2795.

10.1021/cm703689j CCC: $40.75
Published on Web 07/09/2008

Scheme 1. Structure of Multilayer OLED Constituent Materials: TPD (HTL), NPB (HTL), PEDOT (HTL), Alq (EML/ETL), TPD−Si_2, and TPD−$[Si(OMe)_3]_2$

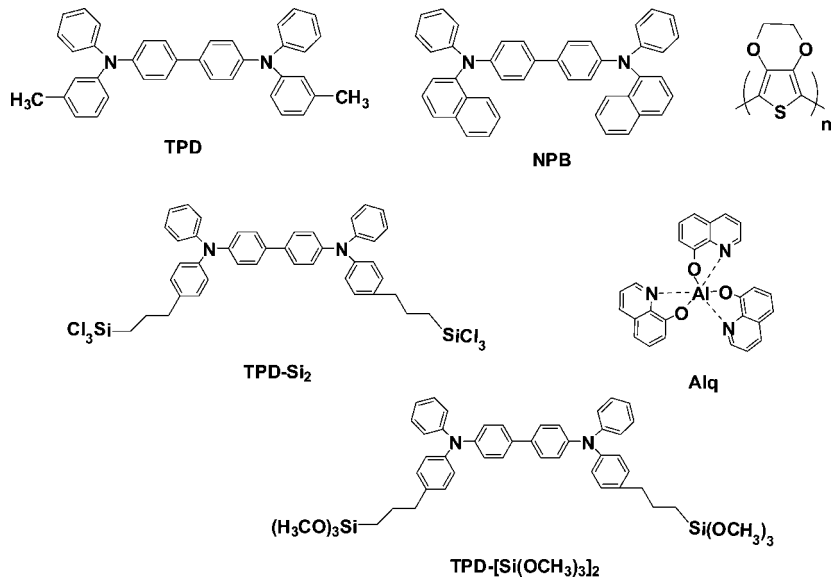

via vacuum deposition. Typical small-molecule HTLs are triarylamine-based materials such as NPB or TPD (Scheme 1), which are known to have appreciable hole-transporting and electron/exciton-blocking capacity because of their relatively high-lying lowest unoccupied molecular orbital (LUMO) levels and large highest occupied molecular orbital (HOMO)−LUMO gaps.

To date, increasing evidence indicates that the anode (usually tin-doped indium oxide, ITO)−HTL interface is crucial to hole injection in a common scenario where ITO−HTL contact rather than HTL bulk mobility limits charge injection.[21–25] To tune the electronic properties at an anode surface has been a crucial issue because electronic profiles at the anode/organic interface strongly affect electron/hole injection fluence and recombination of the charge carriers that are central factors for enhancing OLED efficiency.[9,11,26,27] A variety of interfacial engineering approaches have been applied to the anode−HTL junction, including introduction of π-conjugated polymers,[28] such as polyaniline-camphorsulfonic acid (PANI-CSA)[29,30] and poly(3,4-ethylenedioxythiophene)−poly(styrenesulfonate) (PEDOT−PSS) (Scheme 1),[31–33] copper phthalocyanine,[34,35] organic phosphonic[36,37] and carboxylic acids,[38] a thin layer of platinum,[39] self-assembled polar molecules to manipulate surface dipoles,[40,41] self-assembled siloxanes,[42–44] and plasma treatment of the ITO surface.[45] All of these approaches have nonnegligible effects on hole injection and yield varying degrees of improved device performance in terms of turn-on voltage, luminance, stability, and/or current efficiency. In previous work from this laboratory, we demonstrated that small-molecule OLED performance and durability can be significantly enhanced using triarylamine-based siloxane hole-transporting materials such as TPD−Si_2 (Scheme 1) as an anode hole injection/adhesion interlayer.[8–12,43,44,46–51] (TPD−Si_2 combines the hole-transport capacity of TPD, the covalent-bonding capacity of chlorosilyl/silanol groups, and can enhance OLED hole injection and device durability as

(21) Shen, Y.; Jacobs, D. B.; Malliaras, G. G.; Koley, G.; Spencer, M. G.; Ioannidis, A. *Adv. Mater.* **2001**, *13*, 1234–1238.
(22) Forsythe, E. W.; Abkowitz, M. A.; Gao, Y. *J. Phys. Chem. B* **2000**, *104*, 3948–3952.
(23) Nesch, F.; Forsythe, E. W.; Le, Q. T.; Gao, Y.; Rothberg, L. J. *J. Appl. Phys.* **2000**, *87*, 7973–7980.
(24) Appleyard, S. F. J.; Day, S. R.; Pickford, R. D.; Willis, M. R. *J. Mater. Chem.* **2000**, *10*, 169–173.
(25) Malinsky, J. E.; Jabbour, G. E.; Shaheen, S. E.; Anderson, J. D.; Richter, A. G.; Marks, T. J.; Armstrong, N. R.; Kippelen, B.; Dutta, P.; Peyghambarian, N. *Adv. Mater.* **1999**, *11*, 227–231.
(26) Hatton, R. A.; Willis, M. R.; Chesters, M. A.; Briggs, D. *J. Mater. Chem.* **2003**, *13*, 722.
(27) Lee, J.; Jung, B.-J.; Lee, J.-I.; Chu, H. Y.; Do, L.-M.; Shim, H.-K. *J. Mater. Chem.* **2002**, *12*, 3494.
(28) Gross, M.; Muller, D.; Nothofer, H.; Scherf, U.; Neher, D.; Brauchle, C.; Meerholz, K. *Nature* **2000**, *405*, 661–665.
(29) Yang, Y.; Heeger, A. H. *Appl. Phy. Lett.* **1994**, *64*, 1245–1247.
(30) Carter, S. A.; Angelopoulos, M.; Karg, S.; Brock, P. J.; Scott, J. C. *Appl. Phys. Lett.* **1997**, *70*, 2067–2069.
(31) Brown, T. M.; Kim, J. S.; Friend, R. H.; Cacialli, F.; Daik, R.; Feast, W. J. *Appl. Phys. Lett.* **1999**, *75*, 1679–1681.
(32) Groenendaal, B. L.; Jonas, F.; Freitag, D.; Pielartzik, H.; Reynolds, J. R. *Adv. Mater.* **2000**, *12*, 481–494.
(33) Cao, Y.; Yu, G.; Zhang, C.; Menon, R.; Heeger, A. J. *Synth. Met.* **1997**, *87*, 171–174.
(34) Tadayyon, S. M.; Grandin, H. M.; Griffiths, K.; Norton, P. R.; Aziz, H.; Popovic, Z. D. *Org. Electron.* **2004**, *5*, 157–166.
(35) Mori, T.; Mitsuoka, T.; Ishii, M.; Fujikawa, H.; Taga, Y. *Appl. Phys. Lett.* **2002**, *80*, 3895–3897.
(36) Appleyard, S. F. J.; Day, S. R.; Pickford, R. D.; Willis, M. R. *J. Mater. Chem.* **2000**, *10*, 169–174.
(37) Guo, J.; Koch, N.; Schwartz, J.; Bernasek, S. L. *J. Phys. Chem. B* **2005**, *109*, 3966–3970.
(38) Berlin, A.; Zotti, G.; Schiavon, G.; Zecchin, S. *J. Am. Chem. Soc.* **1998**, *120*, 13453–13460.
(39) Shen, Y.; Jacobs, D. B.; Malliaras, G. G.; Koley, G.; Spencer, M. G.; Ioannidis, A. *Adv. Mater.* **2001**, *13*, 1234–1238.
(40) Ganzorig, C.; Kwak, K. J.; Yagi, K.; Fujihira, M. *Appl. Phys. Lett.* **2001**, *79*, 272–274.
(41) Bruening, M.; Moons, E.; Yaron-Marcovich, D.; Cahen, D.; Libman, J.; Shanzer, A. *J. Am. Chem. Soc.* **1994**, *116*, 2972.
(42) Malinsky, J. E.; Jabbour, G. E.; Shaheen, S. E.; Anderson, J. D.; Richter, A. G.; Marks, T. J.; Armstrong, N. R.; Kippelen, B.; Dutta, P.; Peyghambarian, N. *Adv. Mater.* **1999**, *11*, 227–231.
(43) Cui, J.; Huang, Q.; Wang, Q.; Marks, T. J. *Langmuir* **2001**, *17*, 2051–2054.
(44) Cui, J.; Huang, Q.; Veinot, J. C. G.; Yan, H.; Wang, Q.; Hutchison, G. R.; Richter, A. G.; Evmenenko, G.; Dutta, P.; Marks, T. J. *Langmuir* **2002**, *18*, 9958–9970.
(45) Milliron, D. J.; Hill, I. G.; Shen, C.; Kahn, A.; Schwartz, J. *J. Appl. Phys.* **2000**, *87*, 572–576.

a hole injection/adhesion interlayer.) However, these trichorosilane-based molecules are sensitive to moisture and air. Thus, they are not easily adapted to conventional large-area process conditions, such as roll-to-roll and ink-jet patterning processes.

In this contribution, we report the synthesis, characterization, and implementation of a new interlayer material, TPD−$[Si(OCH_3)_3]_2$, which has relatively air-stable trimethoxysilyl linkers. A robust, smooth, conformal, adherent, and essentially pinhole-free monolayer or multilayer films can be deposited by self-assembly and simple spin-casting this molecule, respectively, via covalent In−O−Si/Sn−O−Si linkages. Both of these approaches afford Alq (tris(8-hydroxyquinolato)aluminum(III), Scheme 1)-based small-molecule OLEDs with superior performance versus devices relying on simple ITO−NPB interfaces without an interlayer and performance comparable to that of TPD−Si_2 interlayer-based OLEDs.

2. Experimental Section

2.1. Materials and Methods. ITO glass sheets (20 Ω/□, rms roughness = 2.5 nm) were purchased from Colorado Concept Coating. All chemical reagents were used as received unless otherwise indicated. All manipulations of air/moisture-sensitive materials were carried out on a dual-manifold Schlenk line or in a nitrogen-filled glovebox. Ether and THF were distilled before use from sodium/benzophenone ketyl. Methylene chloride was distilled before use from calcium hydride. Toluene was dried using activated alumina and Q5 columns and tested with benzyphenone ketyl in ether solution. TPD and Alq were purchased from Sigma-Aldrich and purified via vacuum gradient sublimation. NPB was synthesized according to the literature[52] and was purified by recrystallization followed by vacuum gradient sublimation. The synthesis of TPD−Si_2 was reported elsewhere.[11] NMR spectra were obtained on Varian VXR-400 or 500 MHz NMR instruments. MS analyses were conducted on a Micromass Quattro II triple quadrupole HPLC/MS/MS mass spectrometer. Elemental analyses were carried out by Midwest Microlabs. Cyclic voltammetry was performed with a BAS 100 electrochemical workstation (SAM-coated ITO with ∼1 cm^2 area working electrodes, Ag wire pseudoreference electrode, Pt wire counter electrode, 0.1 M tetrabutylammonium hexafluorophosphate (TBAHFP) in anhydrous MeCN supporting electrolyte, and 0.001 M ferrocene as the internal pinhole probe. Scan rate = 0.1 V/s). TBAHFP was recrystallized from an ethyl acetate/hexanes mixture and dried in vacuo at 100 °C for 10 h. Ferrocene was purchased from Sigma-Aldrich and purified via vacuum gradient sublimation. Atomic force microscopy (AFM) images were obtained on a Nanoscope III AFM under ambient conditions in the contact mode with Si_3N_4 cantilevers. Specular X-ray reflectivity experiments on coated single-crystal Si(111) substrates were performed on the National Research Laboratory X23B beamline at the National Synchrotron Light Source. Data were acquired and analyzed as described previously.[11,44] The thickness of spin-cast films was measured with a Tencor P-10 profilometer. X-ray photoelectron spectroscopy (XPS) measurements were performed at Northwestern University with an Omicron ESCA probe, which was equipped with EA125 energy analyzer. Photoemission was stimulated by a monochromatic Al Kα radiation (1486.6 eV) with the operating power of 300 W, and a low-energy electron flood gun was employed for charge neutralization. Binding energies of spectra were referenced to the C 1s binding energy set at 284.8 eV.

2.2. Synthesis of 4,4′-Bis[(*p*-bromophenyl)phenylamino)]biphenyl (1). To a toluene solution (50 mL) of tris(dibenzyldeneacetone)dipalladium (0.55 g, 0.60 mmol) and bis(diphenylphosphino)ferrocene, (0.50 g, 0.90 mmol) was added 1,4-dibromobenzene (18.9 g, 0.0800 mol) at 25 °C. Following stirring under an N_2 atmosphere for 10 min, sodium *tert*-butoxide (4.8 g, 0.050 mol) and *N*,*N*′-diphenylbenzidine (6.8 g, 0.020 mol) were added. The reaction mixture was then stirred at 90 °C for 12 h, followed by cooling to 25 °C. The reaction mixture was then poured into water and the organic and aqueous layers separated. The aqueous layer was extracted with toluene (3 × 100 mL), and the resulting extracts were combined with the original organic layer. The solvent was removed in vacuo giving a crude product which was purified by chromatography on a silica gel column (6:1 hexane/ethylene chloride eluent) to yield pure **1** as a colorless solid (6.9 g) in 50% yield. ^{1}H NMR ($CDCl_3$): δ 6.99 (d, J = 8.8 Hz, 4H), 7.02−7.16 (m, 10H), 7.28 (t, J = 7.6 Hz, 4H), 7.34 (d, J = 8.8 Hz, 4H), 7.45 (d, J = 8.4 Hz, 4H).

2.3. Synthesis of 4,4′-Bis[(*p*-allylphenyl)phenylamino]biphenyl (2). With the use of standard Schlenk techniques, 1.6 mL (3.5 mmol) of *n*-butyl lithium (2.5 M in hexanes) was added dropwise under inert atmosphere to a stirring ether solution (10 mL) of **1** (1.02 g, 1.58 mmol) while maintaining the temperature at 25 °C. The mixture was stirred for 2 h after which time CuI (0.76 g, 4.0 mmol) was next added. Upon cooling the reaction mixture to 0 °C, allyl bromide (0.60 g, 5.0 mmol) was added in one portion and the mixture stirred for 14 h, followed by quenching with saturated aqueous NH_4Cl solution (100 mL) and extraction with ether (3 × 100 mL). The combined ether extracts were washed with water (2 × 100 mL) and brine (2 × 100 mL) and dried over anhydrous Na_2SO_4. Filtration and removal of solvent in vacuo afforded a yellow oil, which was further purified by chromatography on a silica gel column (4:1 hexane/methylene chloride) to yield 0.63 g of pure **2** as a colorless solid. Yield: 70%. ^{1}H NMR ($CDCl_3$): δ 3.40 (d, J = 10 Hz, 4H), 5.10−5.20 (m, 4H), 6.02 (m, 2H), 6.99−7.10 (m, 2H), 7.10−7.20 (m, 16H), 7.28 (t, J = 7.6 Hz, 4H), 7.46 (d, J = 8.8 Hz, 4H). Anal. Calcd for $C_{42}H_{36}N_2$: C, 88.68; H, 6.39; N, 5.23. Found: C, 87.50; H, 6.35; N, 4.93.

2.4. Synthesis of 4,4′-Bis[(*p*-trimethoxysilylpropylphenyl)-phenylamino]biphenyl (TPD−$[Si(OCH_3)_3]_2$, 3). Under inert atmosphere at 25 °C, a few grains of Cp_2PtCl_2, followed by $HSi(OMe)_3$ (2.15 g, 17.6 mmol), were added to a dry toluene solution (50 mL) of **2** (0.32 g, 0.55 mol), and the reaction mixture was stirred at 80 °C and monitored by NMR until the completion of reaction after 60 h. Removal of the solvent in vacuo yielded a dark-yellow oil, which was triturated with a mixture of 50 mL of anhydrous pentane and 10 mL of anhydrous toluene to yield a solid which was removed by filtration. The filtrate was concentrated in vacuo to yield **3** as a pale-yellow oil. Yield: 94%. ^{1}H NMR ($CDCl_3$): 0.71 (t, J = 7.6 Hz, 4H), 1.73 (t, J = 7 Hz, 4H), 2.60 (br s, 4H), 3.57 (s, 9H), 6.80−7.80 (m, 26H). ^{13}C NMR ($CDCl_3$) δ 9.4, 16.9, 38.9, 50.2, 123.2, 125.7, 126.8, 128.1, 128.8, 129.0, 129.6, 136.4,

(46) Li, W.; Wang, Q.; Cui, J.; Chou, H.; Marks, T. J.; Jabbour, G. E.; Shaheen, S. E.; Kippelen, B.; Pegyhambarian, N.; Dutta, P.; Richter, A. J.; Anderson, J.; Lee, P.; Armstrong, N. *Adv. Mater.* **1999**, *11*, 730.
(47) Cui, J.; Huang, Q.; Veinot, J. G. C.; Yan, H.; Marks, T. *Adv. Mater.* **2002**, *14*, 565–569.
(48) Huang, Q. L.; Cui, J.; Yan, H.; Veinot, J. G. C.; Marks, T. J. *Appl. Phys. Lett.* **2002**, *81*, 3528–3530.
(49) Yan, H.; Huang, Q. L.; Cui, J.; Veinot, J. G. C.; Kern, M. M.; Marks, T. J. *Adv. Mater.* **2003**, *15*, 835–839.
(50) Yan, H.; Huang, Q.; Scott, B. J.; Marks, T. J. *Appl. Phys. Lett.* **2004**, *84*, 3873–3875.
(51) Yan, H.; Lee, P.; Armstrong, N. R.; Graham, A.; Evmenenko, G. A.; Dutta, P.; Marks, T. J. *J. Am. Chem. Soc.* **2005**, *127*, 3172.
(52) Koene, B. E.; Loy, D. E.; Thompson, M. E. *Chem. Mater.* **1998**, *10*, 2235–2250.

Scheme 2. Synthetic Route to TPD−[Si $(OCH_3)_3]_2$

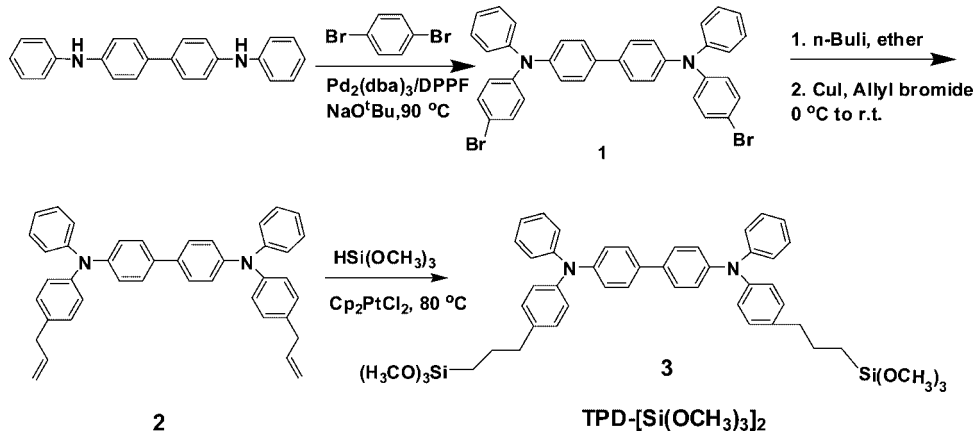

138.2, 143.2, 144.8, 145.9. HRMS calcd for $C_{48}H_{56}N_2O_6Si_2$: 812.37. Found: 812.40.

2.5. Self-Assembly of TPD−[Si$(OCH_3)_3]_2$ on ITO Substrates. ITO substrates were cleaned in an ultrasonic detergent bath, followed by methanol, isopropyl alcohol, and finally acetone. The substrates were subsequently treated in an oxygen plasma cleaner for 1 min to remove any residual organic contaminants. Following strict Schlenk protocol, clean ITO substrates were immersed in a 1.0 mM dry toluene solution of TPD−[Si$(OCH_3)_3]_2$. After heating at ∼90 °C for 4 h, the toluene solution was removed by cannula and the substrates were rinsed with dry toluene (2 × 50 mL) and wet acetone in the ultrasonic bath for 3 min each, followed by transferring to a 120 °C vacuum oven for 2 h to expedite cross-linking. Longer thermal curing yields films with similar properties, and the coating procedure has negligible effects on the measured sheet resistance of the underlying ITO.

2.6. Self-Assembly of TPD−[Si$(OCH_3)_3]_2$ on Silicon Substrates. Silicon(111) substrates (Semiconductor Processing Co.) were subjected to a cleaning procedure as follows. First, the substrates were immersed in "piranha" solution (4:1 H_2SO_4/H_2O_2) at 80 °C for 1 h. After cooling to room temperature, the substrates were rinsed repeatedly with deionized (DI) water followed by an RCA-type cleaning protocol (H_2O/30% H_2O_2/NH_3; 5:1:1 v/v/v; sonicated at room temperature for 40 min). The substrates were finally rinsed with copious amounts of DI water, heated to 125 °C for 15 min, and dried in vacuo. TPD−[Si$(OCH_3)_3]_2$ was then self-assembled onto the clean silicon substrates following the procedure described above for ITO substrates

2.7. Spin-Casting of TPD−[Si$(OCH_3)_3]_2$ on ITO Substrates. A toluene solution of TPD−[Si$(OCH_3)_3]_2$ (4 mg/mL) was spin-coated onto clean ITO substrates at 1500 rpm in air, followed by curing in a vacuum oven at 110 °C for 2 h.[10] To improve the cross-linking reaction of TPD−[Si$(OMe)_3]_2$, another facile method was used. A 95% ethanol−5% water solution was adjusted to pH = 4.5−5.5 with acetic acid. TPD−[Si$(OCH_3)_3]_2$ was added with stirring to yield a 2% final concentration. The aqueous alcohol solution of TPD−[Si$(OCH_3)_3]_2$ was then spin-coated onto the clean ITO surfaces at 1000 rpm in air, followed by curing in a vacuum oven at 110 °C for 2 h.[10,56] Note here that the TPD−[Si$(OCH_3)_3]_2$ solution was distributed evenly on the ITO plate from a syringe with a 0.2 μm HPLC filter and exposed in the air for 5 min before spinning, to optimize hydrolysis and silanol formation. The appropriate concentration of building block solution and the spinning speed was obtained after a few experiments.

2.8. Fabrication of OLED Devices. The bare, precleaned in oxygen plasma ITO films, and modified ITO substrates were loaded into a bell jar deposition chamber housed in a nitrogen-filled glovebox. A typical deposition procedure is as follows: At 1 × 10^{-6} Torr, a 20 nm layer of NPB was first deposited, followed by 60 nm of Alq. Both organic layers were grown at a deposition rate of 2−3 Å/s. Finally, 1 nm of LiF and a 100 nm thick Al cathode were deposited through a shadow mask. This metallic layer was patterned to give four devices, each with an area of 0.10 cm^2. OLED device characterization was carried out with a computer-controlled Keithley 2400 source meter and IL 1700 research radiometer equipped with a calibrated silicon photodetector at 25 °C under ambient atmosphere. Current efficiency was estimated from current density versus voltage and luminance versus current density response characteristics.

2.9. Fabrication of Hole-Only Devices. Bare and modified ITO substrates were loaded into a bell jar deposition chamber housed within a nitrogen-filled glovebox. At a base pressure of 1 × 10^{-6} Torr, NPB (400 nm) was vapor deposited at a rate of ∼3 Å/s, followed by sputter-coating of a 6 nm of Au layer through the same shadow mask employed for the OLED fabrication described above. Single-carrier device assembly was subsequently completed with the masked thermal vapor deposition of Al (150 nm). Device behavior was evaluated using the computer-controlled Keithley 2400 source meter.

3. Results and Discussion

In section 3.1, we discuss the deposition and characterization of self-assembled monolayers (SAMs) or spin-coated films of TPD−[Si$(OMe)_3]_2$ on glass/ITO substrates. In section 3.2, SAMs or spin-coated films of TPD−[Si$(OMe)_3]_2$ are used as ITO anode−NPB interlayers, and the effect on OLED electroluminescence (EL) response compared to SAMs or spin-coated films of TPD−Si_2, having −$SiCl_3$ linkers, and which is much more reactive than −Si$(OMe)_3$, is analyzed here. It will be seen that Alq-based small-molecule OLEDs with SAMs or spin-coated films of TPD−[Si$(OMe)_3]_2$ interlayers exhibit superior performance versus devices relying on simple ITO−NPB interfaces without an interlayer, and performance comparable to that of TPD−Si_2 interlayer-based OLEDs.

3.1. Deposition and Characterization of TPD−[Si$(OMe)_3]_2$ on ITO Substrate. *3.1.1. Anhydrous and Hydrolytic Depositions of TPD−[Si$(OMe)_3]_2$ on ITO Substrate.* The synthetic pathway to TPD−[Si$(OMe)_3]_2$ is summarized in Scheme 2, while detailed procedures and characterization data are presented in the Experimental Section. Utilizing a self-limiting, anhydrous solution-based

Scheme 3. Mechanisms of ITO Surface Modification by Trimethoxysilane Reagents to Form Thin Film HTL Materials[a]

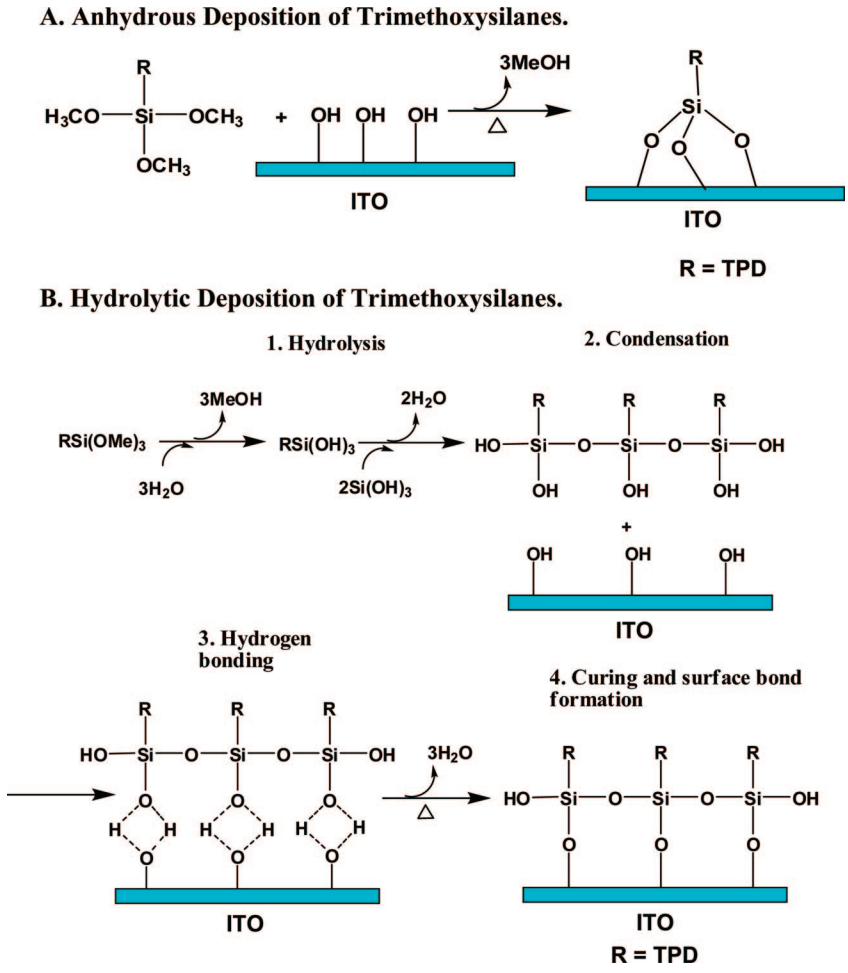

[a] (A) Anhydrous deposition; (B) hydrolytic deposition.

chemisorption process, TPD−$[Si(OMe)_3]_2$ is self-assembled onto hydrophilic glass/ITO substrate surfaces with nanoprecise control in thickness. As illustrated in Scheme 3, clean ITO-coated glass surface possesses hydroxyl functionalities which are reactive toward methoxysilanes, thereby affording covalent binding of the silanes to the surface.[53–55] The process of anhydrous deposition is described in Scheme 3A,[56] through which a monolayer of siloxane (∼1.75 nm) forms. For organo−SiX_3 precursors, approximately three bonds are formed from each silicon to hydroxylated surfaces.[53–55] Further exposure to air and moisture in the following wet acetone rinse hydrolyzes any unreacted methoxysilyl groups. Subsequent thermal curing facilitates formation of cross-linked siloxane networks, resulting in a thin layer consisting of hole-transporting moieties covalently anchored to the ITO surface.

Spin-casting TPD−$[Si(OMe)_3]_2$ from toluene solution or acidic aqueous alcohol solutions blended with acetic acid affords thicker films (∼40 nm, measured by a profilometer) on glass/ITO substrates (Scheme 3B),[56] which is different from the anhydrous deposition described above, given that the spin-coating parameters such as solution concentration and spinning speed are carefully controlled (see the Experimental Section for details). During the hydrolytic deposition, the TPD−$[Si(OMe)_3]_2$ methoxy groups are hydrolyzed to form silanol-containing species. This reaction mode of TPD−$[Si(OMe)_3]_2$ likely involves four steps: (1) hydrolysis, (2) condensation, (3) hydrogen bonding, and (4) surface bond formation.[56] Initially, hydrolysis of the Si−OCH_3 groups occurs. Water for hydrolysis may come from several sources. It may be added, it may be present on the substrate surface, or it may come from the atmosphere. Condensation to oligomers follows. The oligomers then hydrogen bond with OH groups of the substrate. Finally, during drying or curing, a covalent linkage is formed to the substrate with concomitant loss of water. Although described sequentially, these reactions can occur simultaneously after the initial hydrolysis step. The microstructural characterization of these layers is presented below.

3.1.2. Characterization of TPD−$[Si(OMe)_3]_2$-Derived Films by Advancing Aqueous Contact Angles and X-ray Photoelectron Spectroscopy. Aqueous advancing contact angles were measured before and after self-assembly/spin-casting. Because the hydroxyl groups of the oxide layer create a hydrophilic surface, bare ITO exhibits a very low contact

(53) Ulman, A. *Chem. Rev.* **1996**, *96*, 1533–1554.
(54) Jeon, N. L.; Nuzzo, R. G.; Xia, Y.; Mrksich, M.; Whitesides, G. M. *Langmuir* **1995**, *11*, 3024–3026.
(55) Ulman, A. *Thin Solid Films* **1996**, *273*, 48–53.
(56) (a) Silane Coupling Agents: Connecting Across Boundaries. *Gelest Inc. Catalog*, Gelest, Inc.: Morrisville, PA, 2001; pp 1−20. (b) Plueddemann, E. In *Silane Coupling Agents*, 2nd ed.; Plenum Press: New York, 1991. (c) Witucki, G. L. *J. Coat. Technol.* **1993**, *65*, 57–60.

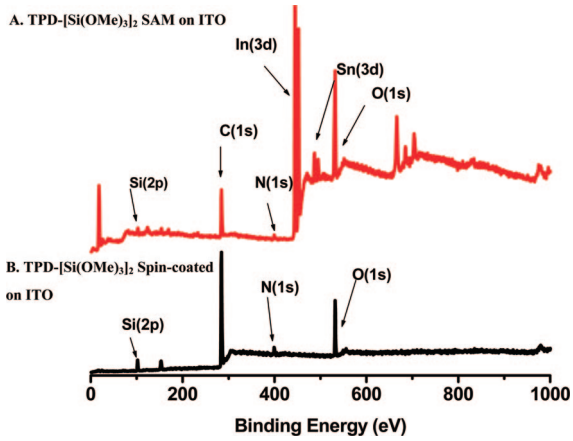

Figure 2. XPS spectra of a TPD−[Si(OMe)$_3$]$_2$-derived SAM and spin-coated film on glass/ITO substrates.

angle value ($\theta \leq 15°$); however, after TPD−[Si(OMe)$_3$]$_2$ self-assembly or spin-casting, relatively high values ($\theta = 77°$ for SAM-modified ITO and $\theta = 85°$ for spin-coated film-modified ITO) are observed, indicating that the ITO surfaces become hydrophobic. In addition to these contact angle measurements, an XPS study was also performed to investigate the surface atomic composition. Figure 2 shows the XPS spectra of the TPD−[Si(OMe)$_3$]$_2$-derived SAM (Figure 2A) and spin-coated film (Figure 2B) on ITO. Two new features characteristic of Si (2p) at 101.0 eV and N (1s) at 400 eV are attributable to TPD−[Si(OMe)$_3$]$_2$ hydrolysis products. Note here that In and Sn peaks can no longer be detected on the spin-coated TPD−[Si(OMe)$_3$]$_2$ films, since the thickness of the spin-casting film is significantly beyond 10 nm. Note that standard XPS techniques measure the kinetic energies and numbers of electrons escaping from the upper 1−10 nm of the material being analyzed.[57]

3.1.3. Characterization of TPD−[Si(OMe)$_3$]$_2$-Derived Films by Specular X-ray Reflectivity and Profilometry. X-ray reflectivity (XRR) measurements on TPD−[Si(OMe)$_3$]$_2$ SAMs deposited on single-crystal Si(111) substrates yield a thickness of 1.75 nm (close to the value of ∼1.45 nm estimated by an approximate AM1-level calculation), suggesting that most TPD−[Si(OMe)$_3$]$_2$ molecules are chemisorbed on the substrate in an approximately "upright" orientation. The thicknesses of TPD−[Si(OMe)$_3$]$_2$ films spin-cast from toluene solution or from the aqueous alcohol + acetic acid blend solution are ∼37 and ∼43 nm, respectively, determined by profilometry measurements. Similarly, the thickness of a spin-cast TPD−Si$_2$ film is around 35 nm.

3.1.4. Characterization of TPD−[Si(OMe)$_3$]$_2$-Derived Films by Atomic Force Microscopy. Tapping mode AFM imaging was carried out on three spots randomly chosen on each TPD−[Si(OMe)$_3$]$_2$-derived film on ITO substrates, self-assembled or spin-cast from toluene solution or the aqueous alcohol + acetic acid blend solution, respectively. Uniform films with no evidence of cracks or pinholes are observed over a 5 × 5 μm^2 scan area (Figure 3). The rms roughness is 2.0 nm for the TPD−[Si(OMe)$_3$]$_2$ SAM and 2.8 and 1.5 nm, respectively, for spin-coated TPD−[Si(OMe)$_3$]$_2$ films from toluene solution and from the aqueous alcohol + acetic acid blend solution, as compared to bare ITO substrates which have an rms roughness of 2.5 nm.

3.1.5. Characterization of TPD−[Si(OMe)$_3$]$_2$-Derived Films by Cyclic Voltammetry: Redox Property Assessment by Cyclic Voltammetry. Glass/ITO substrates covered with TPD−[Si(OMe)$_3$]$_2$-derived SAMs or spin-coated films, a silver wire, and a Pt wire were used as the working electrode, reference electrode, and counter electrode, respectively, in a 0.1 M acetonitrile solution of TBAHFP as the electrolyte without ferrocene. The cyclic voltammetry plots obtained at a scan rate of 0.1 V/s are shown in Figure 4A. The cyclic voltammetry of self-assembled or spin-coated TPD−[Si(OMe)$_3$]$_2$ films on ITO electrodes indicates that they are electroactive, capable of efficient hole transport, and electrochemically stable. The densely cross-linked nature of TPD−[Si(OMe)$_3$]$_2$ films is evident in the relatively large separation of oxidative and reductive peaks (250 mV), suggesting kinetically hindered oxidation/reduction processes with retarded counterion mobility.[58] Also, the full widths at half-height of oxidative and reductive waves at the sweep rate of 0.1 mV/s are 423 and 235 mV, respectively, which suggest the heterogeneity in the N environments.[63]

Integration of the oxidative peak area and assuming two electron oxidation/reduction events per molecular unit yields a monolayer surface coverage of 3.5 × 10^{-10} mol/cm^2 for the TPD−[Si(OMe)$_3$]$_2$ SAM.[58] Analogously, a close-packed monolayer of ferrocene dicarboxylic acid adsorbed on ITO yields a 4.0 × 10^{-10} mol/cm^2 surface coverage.[59] In addition, the apparent surface coverages of spin-coated TPD−[Si(OMe)$_3$]$_2$ films from the toluene solution and aqueous alcohol + acetic acid blend solution are 6.1 × 10^{-9} and 7.5 × 10^{-9} mol/cm^2, respectively, which indicate the formation of thickness beyond monolayer dimensions in these spin-coated films. The higher apparent surface coverage of the spin-coated TPD−[Si(OMe)$_3$]$_2$ films from aqueous alcohol + acetic acid blend solution than from toluene solution suggests a qualitatively different cross-linking pattern within the latter films, allowing a greater extent of oxidation.

3.1.6. Characterization of TPD−[Si(OMe)$_3$]$_2$-Derived Films by Cyclic Voltammetry: Pinhole Assessment by Ferrocene Cyclic Voltammetry. To examine the present TPD−[Si(OMe)$_3$]$_2$-derived films for pinholes over the entire ITO substrate area (1 cm^2), cyclic voltammetry experiments using ferrocene as an internal redox probe were carried out.[60] Here the self-assembled and spin-coated siloxane film-coated ITO substrates were used as working electrodes with bare ITO substrates used as references to calibrate the ferrocene redox potential for each measurement. The results are shown in Figure 4B. The ferrocene oxidation peak potential is ∼1.0 V with the bare ITO substrate as the working electrode and is shifted to 1.8 V (TPD−[Si(OMe)$_3$]$_2$ SAM), 2.4 V (spin-

(57) (a) Crist, B. V. In *Handbooks of Monochromatic XPS Spectra*; Crist, B. V., Ed.; XPS International LLC: Mountain View, CA, 2004; Vols. *1*−*5*. (b) Grant, J. T.; Briggs, D. In *Surface Analysis by Auger and X-ray Photoelectron Spectroscopy*; Grant, J. T., Briggs, D., Eds.; IM Publications: Chichester, U.K., 2003.

(58) Murray, R. W. In *Molecular Design of Electrode Surfaces*; Murray, R. W., Ed.; Techniques of Chemistry; Wiley: New York, 1992; Vol. 22, pp 1−158.

(59) Donley, C.; Dunphy, D.; Paine, D.; Carter, C.; Nebesny, K.; Lee, P.; Alloway, D.; Armstrong, N. R. *Langmuir* **2002**, *18*, 450–457.

(60) DuBois, C. J., Jr.; McCarley, R. L. *J. Electroanal. Chem.* **1998**, *454*, 99–105.

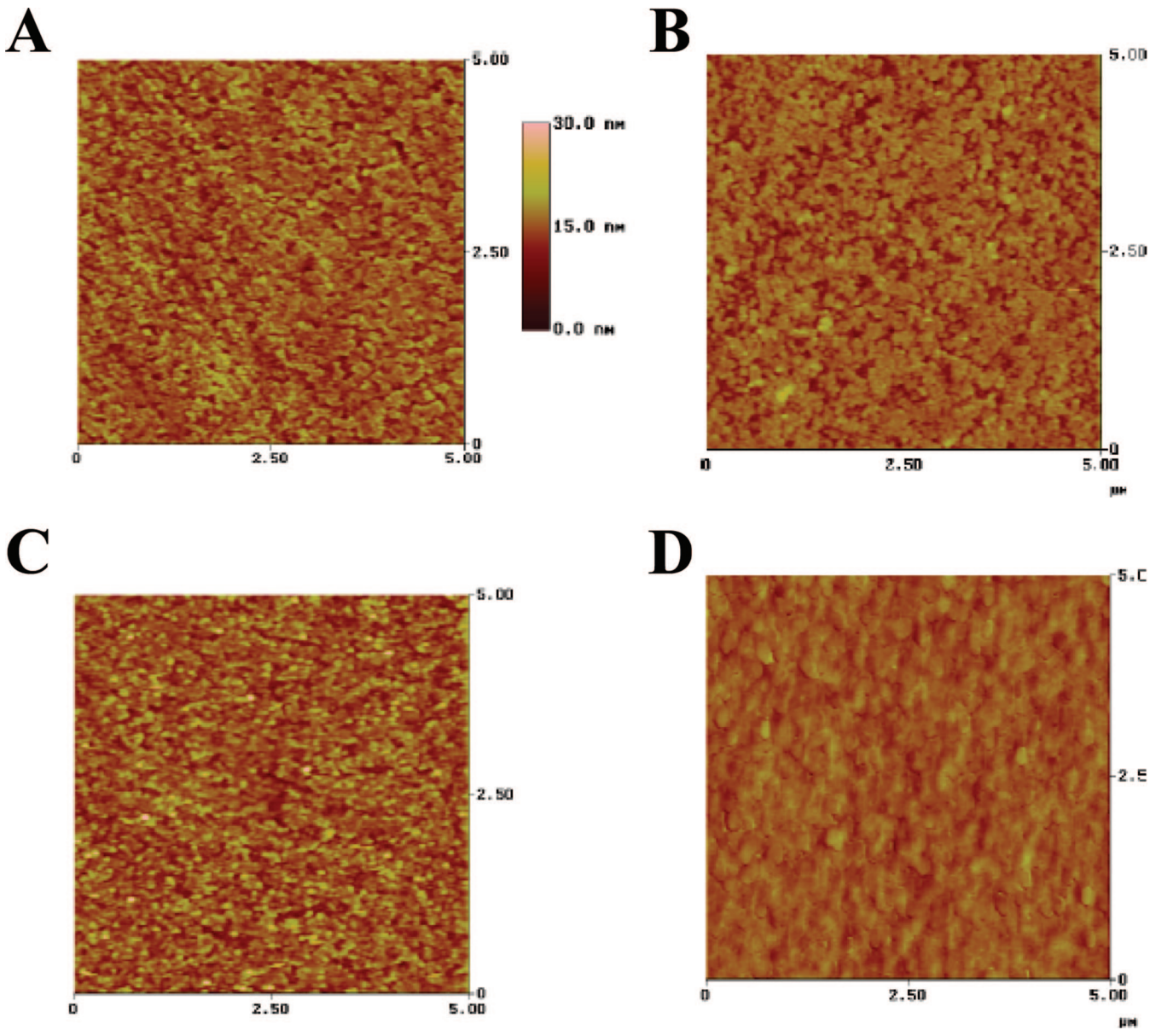

Figure 3. Tapping mode AFM images of self-assembled or spin-cast TPD−$[Si(OMe)_3]_2$-derived films, deposited from toluene solution or aqueous alcohol + acetic acid blend solution on ITO substrates. (A) Bare ITO; rms roughness = 2.5 nm. (B) TPD−$[Si(OMe)_3]_2$ SAM on ITO; rms roughness = 2.0 nm. (C) TPD−$[Si(OMe)_3]_2$ spin-coated film from toluene solution on ITO; rms roughness = 2.8 nm. (D) TPD−$[Si(OMe)_3]_2$ spin-coated film from aqueous alcohol + acetic acid blend solution on ITO; rms roughness = 1.5 nm.

coated TPD−$[Si(OMe)_3]_2$ film from toluene solution), and 2.75 V (spin-coated TPD−$[Si(OMe)_3]_2$ film from aqueous alcohol + acetic acid blend solution), respectively, with the self-assembled and spin-coated film-coated ITO substrates as working electrodes. The lack of significant current flow near the formal oxidation potential of ferrocene indicates an inhibition of ferrocene oxidation, resulting from conformal and largely pinhole-free film coverage of the ITO. As the triarylamine oxidation potentials are reached, an electrocatalytic current response is observed, indicating that ferrocene is oxidized at an essentially diffusion-controlled rate, meaning that facile triarylamine group oxidation at the ITO−HTL interface (hole injection) and rapid hole migration (presumably accompanied by counteranion migration) through the nanoscopic film occurs such that ferrocene oxidation takes place at the film−solution interface.[61,62]

The reduction of the ferricenium cation on the return sweep is partially blocked by the TPD−$[Si(OMe)_3]_2$ SAM, and more completely blocked by the spin-coated TPD−$[Si(OMe)_3]_2$ films, suggesting that the latter films are somewhat more pinhole-free.[63] The larger separations of ferrocene oxidative and reductive peak potentials at the self-assembled and spin-coated siloxane film-coated ITO electrodes versus on the bare ITO ones (2.8 V, spin-coated TPD−$[Si(OMe)_3]_2$ film from aqueous alcohol + acetic acid blend solution; 2.1 V, spin-coated TPD−$[Si(OMe)_3]_2$ film from toluene solution; 1.30 V, TPD−$[Si(OMe)_3]_2$ SAM; 0.4 V, bare ITO) may also indicate that in the redox processes,

(61) Immoos, C. E.; Chou, J.; Bayachou, M.; Blair, E.; Greaves, J.; Farmer, P. J. *J. Am. Chem. Soc.* **2004**, *126*, 4934–4942.
(62) Nowall, W. B.; Kuhr, W. G. *Anal. Chem.* **1995**, *67*, 3583–3588.
(63) Inzelt, G. In *Electroanalytical Chemistry*; Bard, A. J., Rubenstein, I., Eds.; Marcel Dekker: New York, 1994; Vol. 18, pp 90−134.

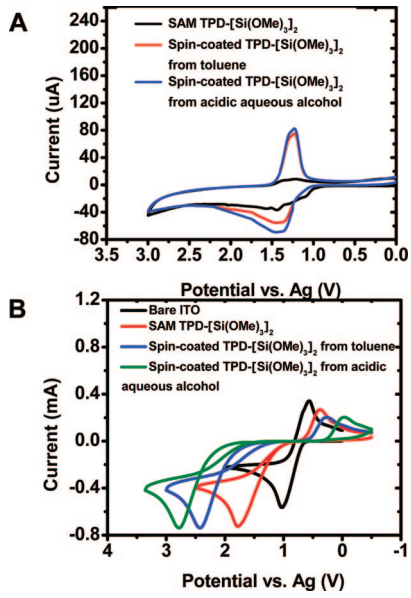

Figure 4. (A) Cyclic voltammetry of TPD−$[Si(OMe)_3]_2$-derived SAM and spin-coated films on glass ITO with 0.1 M TBAHFP electrolyte at a 0.1 V/s scan rate. (B) Cyclic voltammetry of SAM and spin-coated TPD−$[Si(OMe)_3]_2$ films on ITO with 1 mM ferrocene as an internal probe in 0.1 M TBAHFP electrolyte at a 0.1 V/s scan rate. The features shown are the electrochemical signatures of ferrocene, used here as a pinhole probe.

counterion penetration, and diffusion in the siloxane films is retarded, presumably due to the densely packed, cross-linked networks.[64–67] It is likely that the spin-coated TPD−$[Si(OMe)_3]_2$ films from aqueous alcohol + acetic acid blend solution, due to the water and acetic acid in the solvent, which accelerate hydrolysis of the methoxysilane groups,[56] are more heavily cross-linked compared to the spin-coated TPD−$[Si(OMe)_3]_2$ films from toluene solution, resulting in somewhat more densely packed films.

3.2. Self-Assembled and Spin-Cast TPD−$[Si(OMe)_3]_2$ Films in OLEDs. *3.2.1. Applying TPD−[Si(OMe)$_3$]$_2$ SAM as ITO Anode−NPB Interlayer.* Self-assembled TPD−$[Si(OMe)_3]_2$-derived and TPD−Si_2-derived monolayers were applied as interlayers between the ITO anode and a conventional vapor-deposited NPB HTL in OLEDs having structures ITO/HTL SAM/NPB (20 nm)/Alq (60 nm)/LiF (1 nm)/Al (100 nm). Insertion of these interlayers between the anode and the NPB HTL dramatically enhances OLED EL response compared to devices without the interlayers (Figure 5 and Table 1). As compared to OLEDs using an NPB-only HTL, which is in direct contact with the ITO anodes, the maximum light output is enhanced by an order of magnitude both for TPD−$[Si(OMe)_3]_2$-based and TPD−Si_2-based devices: ∼1900 cd/m^2 (NPB-only) → 26 500 cd/m^2 (TPD−$[Si(OMe)_3]_2$/NPB) and 25 900 cd/m^2 (TPD−Si_2/NPB), respectively. Likewise, the maximum current efficiency is increased by a factor of ∼4× for both devices: 4.41 cd/A (TPD−$[Si(OMe)_3]_2$/NPB) and 4.10 cd/A (TPD−Si_2/NPB) versus 1.17 cd/A (NPB alone). Also, TPD−$[Si(OMe)_3]_2$ and TPD−Si_2 SAM-based OLEDs have lower turn-on and operating voltages. For instance, the operating voltage at 300 cd/m^2, a standard brightness for displays, is 6.1, 6.3, and 8.0 V for TPD−$[Si(OMe)_3]_2$/NPB, TPD−Si_2/NPB, and NPB-only, respectively. These results indicate a substantial increase in hole injection via ITO anode−NPB HTL interfacial modification.

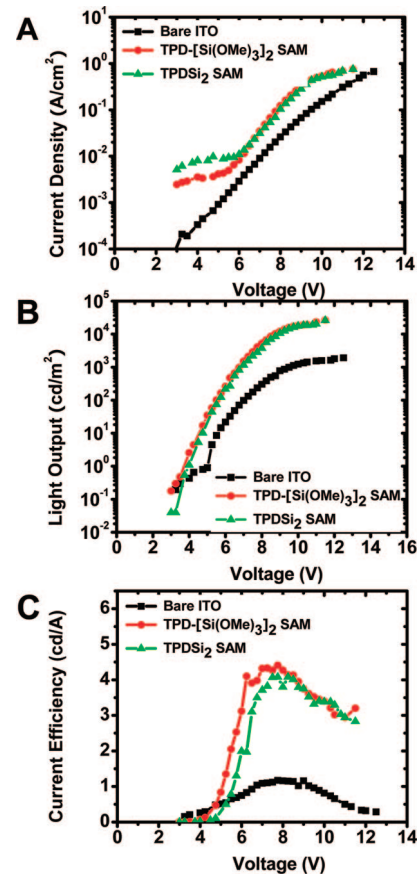

Figure 5. Responses of OLEDs having the structures ITO/HTL SAM/NPB (20 nm)/Alq (60 nm)/LiF (1 nm)/Al (100 nm), HTL SAM = TPD−$[Si(OMe)_3]_2$ SAM, and TPD−Si_2 SAM: (A) current density vs voltage; (B) luminance vs voltage; (C) current efficiency vs voltage.

In the anhydrous toluene deposition of TPD−$[Si(OMe)_3]_2$-derived SAMs, a siloxane monolayer forms on the ITO surface via covalent bonds, a presumably very similar SAM-forming process to that undergone by the trichlorosilane analogue, TPD−Si_2. Indeed, the TPD−$[Si(OMe)_3]_2$ SAM-based devices exhibit almost identical EL response to the TPD−Si_2 SAM-based devices, which can be seen in Figure 5. The substantial OLED EL response enhancement obtained by inserting the siloxane nanostructures between the ITO anode and the NPB HTL, compared to ITO/NPB, can be explained based on the current understanding of ITO anode−HTL interfacial function.[8–12] We propose that the TPD−$[Si(OMe)_3]_2$- and TPD−Si_2-derived materials as ITO anode−NPB interlayers increase hole injection principally by (1) reducing the hole injection barrier from the ITO anode to NPB (HOMO ∼ 5.5 eV) by providing an energy-mediating "step", as shown in Scheme 4; (2) enhancing ITO anode−NPB interfacial cohesion via eliminating the surface

(64) Napper, A. M.; Liu, H. Y.; Waldeck, D. H. *J. Phys. Chem. B* **2001**, *105*, 7699–7707.
(65) Nahir, T. M.; Clark, R. A.; Bowden, E. F. *Anal. Chem.* **1994**, *66*, 2595–2598.
(66) Forster, R. J. *Inorg. Chem.* **1996**, *35*, 3394–3403.
(67) Richardson, J. N.; Rowe, G. K.; Carter, M. T.; Tender, L. M.; Curtin, L. S.; Peck, S. R.; Murray, R. W. *Electrochim. Acta* **1995**, *40*, 1331–1338.

Table 1. OLED EL Response Data for Devices Having the Structure ITO Anode/Interlayer/NPB/Alq/LiF/Al[a]

HTL	TPD−SiOMe SAM	TPD−Si_2 SAM	TPD−SiOMe (spin-coated-1)	TPD−SiOMe (spin-coated-2)	TPD−Si_2 (spin-coated)	NPB-only
max luminance (cd/m^2)	∼26 500	∼25 900	∼28 900	∼32 800	∼29 800	∼1900
max current efficiency (cd/A)	4.41	4.10	5.71	5.8	5.55	1.17
turn-on voltage (V)	4.0	4.0	7.25	4.25	3.7	5.1
operating voltage at 300 cd/m^2 (V)	6.1	6.3	10.4	7.0	6.8	8.0

[a] The interlayer is TPD−$[Si(OMe)_3]_2$ SAM, a TPD−Si_2 SAM, a spin-cast TPD−$[Si(OMe)_3]_2$ from toluene solution, a spin-cast TPD−$[Si(OMe)_3]_2$ from aqueous alcohol + acetic acid blend solution, or a spin-cast TPD−Si_2 film.

Scheme 4. Energy Diagram for the Electrodes and OLED Organic Layers Utilized in This Study (Data Taken from the Literature)

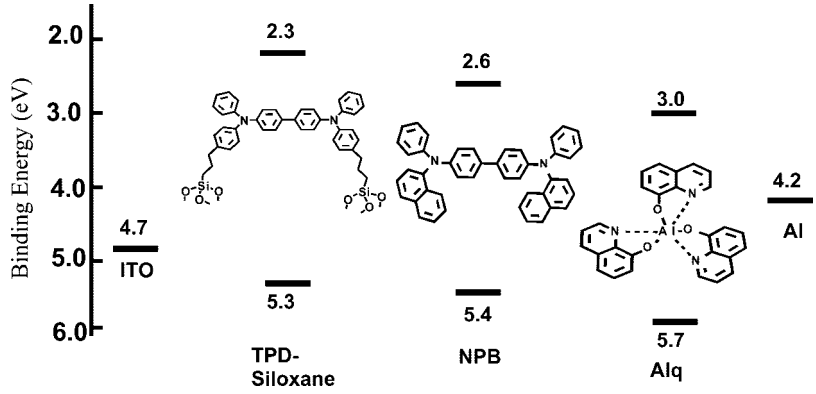

energy mismatch,[44] and creating more intimate ITO anode−HTL physical and electrical contact;[68] (3) contributing to electron-blocking/confinement effects[69] in conjunction with NPB.

3.2.2. Applying Spin-Coated TPD−$[Si(OMe)_3]_2$ Films as ITO Anode−NPB Interlayers. Spin-casting TPD−$[Si(OMe)_3]_2$ layers onto ITO anodes, followed by vapor deposition of NPB, was also investigated as an alternative approach to applying this arylaminomethoxysilane as the anode−NPB interlayer. To assess the properties of the different TPD−$[Si(OMe)_3]_2$ interlayers spin-coated from different solutions and to allow the comparison with spin-coated TPD−Si_2 interlayers in EL devices, we fabricated OLEDs having three different configurations, where SC = spin-coated: ITO/SC-TPD−$[Si(OMe)_3]_2$ cast from toluene solution//NPB/Alq/LiF/Al (device 1), ITO/SC-TPD−$[Si(OMe)_3]_2$ cast from aqueous alcohol + acetic acid blend solution/NPB/Alq/LiF/Al (device 2), and ITO/SC-TPD−Si_2 cast from toluene solution/NPB/Alq/LiF/Al (device 3). The EL response metrics of current density, luminance, and current efficiency versus operating voltage for these devices are compared in Figure 6 and Table 1. Again, enhanced EL response is observed versus that of OLEDs without interlayers and versus devices fabricated with SAMs as ITO anode−HTL interlayers: maximum light output, ∼28 900 cd/m^2 (device 1), ∼32 800 cd/m^2 (device 2), ∼29 800 cd/m^2 (device 3) versus ∼26 500 cd/m^2 (TPD−$(Si(OMe)_3)_2$ SAM), ∼25 900 cd/m^2 (TPD−Si_2 SAM), ∼1900 cd/m^2 (NPB-only); maximum current efficiencies, 5.71 cd/A (device 1), 5.8 cd/A (device 2), 5.5 cd/A (device 3) versus 4.41 cd/A (TPD−$(Si(OMe)_3)_2$ SAM), 4.1 cd/A (TPD−Si_2 SAM), 1.17 cd/A (NPB-only). The improved EL response of spin-coated siloxane film-based OLEDs versus that of OLEDs without interlayers can be explained in the same way as described above for the OLEDs with SAM interlayers. The devices with spin-coated interlayers exhibit greater maximum light output and maximum current efficiency than OLEDs with SAM interlayers, suggesting more effective electron-blocking properties for the ∼35−45 nm thick spin-coated interlayers versus that of self-assembled monolayers with only ∼1−2 nm thickness.[49–51]

The relatively high turn-on voltages in devices having the TPD−$[Si(OMe)_3]_2$ interlayers spin-coated from toluene solution can be seen in Figure 6 and may reflect ITO anode−siloxane film contact differences and incomplete intermolecular cross-linking in the siloxane network because of the less reactive trimethoxysilyl functional groups. This increased turn-on voltage effect is resolved in device 2, in which the TPD−$[Si(OMe)_3]_2$ interlayer was spin-coated from a aqueous alcohol + acetic acid blend solution. The turn-on voltage is 4.25 V for device 2, which is about 3 V less than that for device 1, 7.25 V. The result argues that denser cross-linking of the methoxysilane with the ITO surface and intermolecular cross-linking within the TPD−$[Si(OMe)_3]_2$ siloxane network is expedited by the water and acetic acid, consistent with the film redox properties and pinhole assays by cyclic voltammetry as described above. The enhancement of maximum luminance and current efficiency in device 2 indicates increased hole injection efficiency via increased ITO anode−HTL physical/electrical/chemical contact. This effect was investigated further by fabricating hole-only devices with structures of ITO/SC-TPD−$(Si(OMe)_3)_2$ siloxanes/NPB (400 nm)/Au (6 nm)/Al (120 nm) (Figure 7). Because of the high work function of gold (5.2 eV), electron injection from the Al cathode into NPB is largely blocked so that hole currents dominate the charge transport in the above devices. Because the only difference in the two types of hole-only devices is in the spin-coated TPD−$[Si(OMe)_3]_2$ films, the results clearly

(68) Cahen, D.; Hodes, G. *Adv. Mater.* **2002**, *14*, 789–798.
(69) Yan, H.; Scott, B. J.; Huang, Q.; Marks, T. J. *Adv. Mater.* **2004**, *16*, 1948–1953.

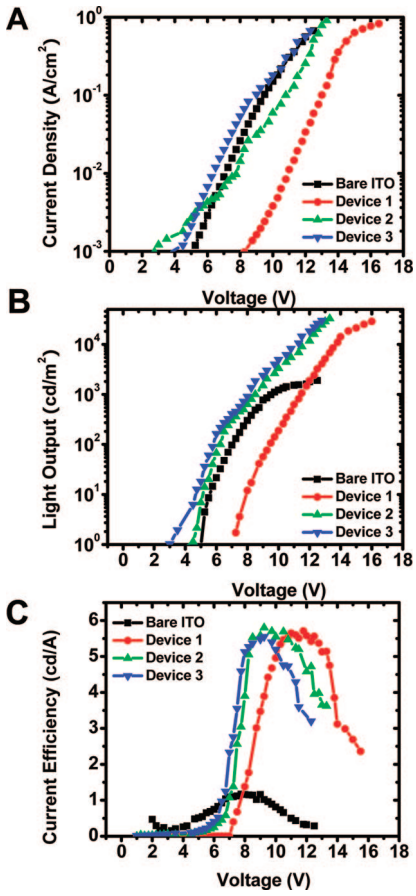

Figure 6. Responses of OLEDs having the structures ITO/spin-coated-TPD−$[Si(OMe)_3]_2$ from toluene solution/NPB (20 nm)/Alq (60 nm)/LiF (1 nm)/Al (100 nm) (device 1), ITO/spin-coated-TPD−$[Si(OMe)_3]_2$ from aqueous alcohol + acetic acid blend solution/NPB (20 nm)/Alq (60 nm)/LiF (1 nm)/Al (100 nm) (device 2), and ITO/spin-coated-TPD−Si_2 from toluene solution/NPB (20 nm)/Alq (60 nm)/LiF (1 nm)/Al (100 nm) (device 3): (A) current density vs voltage; (B) luminance vs voltage; (C) current efficiency vs voltage.

reveal the significant hole injection enhancement by modifying the anode with the spin-coated TPD−$[Si(OMe)_3]_2$ films from the aqueous alcohol + acetic acid blend solution. For example, hole current densities at 20 V are ~0.00004 A/cm^2 (bare ITO) < ~0.0054 A/cm^2 (hole-only device 1) < ~0.015 A/cm^2 (hole-only device 2). The slightly higher turn-on voltage of device 2, 4.25 V, versus that of OLEDs with spin-coated TPD−Si_2-derived interlayers, 3.75 V, is likely due to the greater thickness of spin-coated TPD−$[Si(OMe)_3]_2$ films (~43 nm) from the aqueous alcohol + acetic acid blend solutions compared to TPD−Si_2 films spin-coated from toluene solution with ~35 nm thickness.[10]

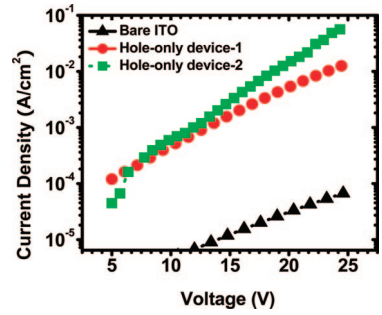

Figure 7. Evaluation of hole injection properties of anode spin-coated functionalization layers, comparing the *I*−*V* response for hole-only devices having the structure ITO/spin-coated siloxane/NPB (400 nm)/Au (6 nm)/Al (120 nm). Spin-coated siloxane = SC-TPD−$[Si(OMe)_3]_2$ from toluene solution (hole-only device 1) and SC-TPD−$[Si(OMe)_3]_2$ from aqueous alcohol + acetic acid blend solution (hole-only device 2).

4. Conclusions

An arylaminotrimethoxysilane functionalized hole-transporting triphenylamine (TPD−$[Si(OMe)_3]_2$) was synthesized and can be self-assembled or spin-coated onto ITO surfaces, enhancing ITO−HTL contact via robust covalent bonding. Various aspects of the SAM and multilayer cross-linked siloxane films were characterized, and OLED devices based on SAM and spin-coated multilayer film-modified glass/ITO substrates were fabricated. The unique contact effects result in dramatic OLED device performance enhancement compared to that of devices without an interlayer. It is also demonstrated here that the cross-linking reaction between TPD−$[Si(OMe)_3]_2$ and ITO substrates as well as the intermolecular cross-linking within the TPD−$[Si(OMe)_3]_2$ siloxane network can be expedited by the presence of water and acetic acid in aqueous alcohol + acetic acid blend spin-coating solutions. The new relatively air-stable interlayer material developed here represents a effective approach to fabricating OLEDs with high brightness (maximum ~32 800 cd/m^2), low operating voltage (~7 V at 300 cd/m^2), and high current efficiency (~5.8 cd/A) and should be suitable for real-world large-area coating conditions, such as roll-to-roll and ink-jet patterning processes.

Acknowledgment. We thank Agiltron Inc. for support of this research. Characterization facilities were provided by the Northwestern MRSEC (NSF Grant DMR-0520513). We thank Dr. G. A. Evmenenko for X-ray reflectivity measurements. We also thank Drs. Q. Wang and Q. Huang for the helpful discussions.

CM703689J